An Investigation into Microlens Array Based Light Field Display for Vision Aberration Correction and Applications to Virtual Reality

Luxin Yang

Electrical Engineering and Computer Sciences
University of California at Berkeley

Technical Report No. UCB/EECS-2020-27
http://www2.eecs.berkeley.edu/Pubs/TechRpts/2020/EECS-2020-27.html

May 1, 2020

Acknowledgement

I want to thank my advisor Prof. Brian A. Barsky for the guidance throughout the work during my Master's research as well as introducing me to the fun world of optometry and vision science. I want to thank Prof. Austin Roorda and Prof. Martin Banks for the courses I took in vision science, which provide great helps in my graduate research.
I thank Prof. Ren Ng and Prof. Laura Waller for being my committee members and giving me so many suggestions in the thesis writing. They also taught the first computational imaging class when I came to Berkeley. The BCCI talks every week are inspiring and benefit me a lot in research.
I would also like to thank my mentor Dr. Ward Lopes and Dr. Fu-chung Huang during my internship at Nvidia, as they are my role models of being a researcher.

An Investigation into Microlens Array Based Light Field Display for Vision Aberration Correction and Applications to Virtual Reality

by

Luxin Yang

A thesis submitted in partial satisfaction of the

requirements for the degree of

Master of Science

in

Computer Science

in the

Graduate Division

of the

University of California, Berkeley

Committee in charge:

Professor Brian A. Barsky, Chair
Professor Yi-Ren Ng
Professor Laura Waller

Spring 2018

An Investigation into Microlens Array Based Light Field Display for Vision Aberration Correction and Applications to Virtual Reality

Abstract

An Investigation into Microlens Array Based Light Field Display for Vision Aberration Correction and Applications to Virtual Reality

by

Luxin Yang

Master of Science in Computer Science

University of California, Berkeley

Professor Brian A. Barsky, Chair

Recent studies have indicated that an increasing number of humans are experiencing refractive visual aberrations. Typically, humans correct optical aberrations by wearing eyeglasses, contact lenses, or undergoing refractive surgeries, but these methods have downsides. Eyeglasses and contact lenses are often inconvenient or uncomfortable for constant usage, and the latter can additionally cause irritation and infection due to surface contact. Refractive surgeries carry the risk of severe side effects such as blurred distance vision and dry eyes. These traditional correcting methods also have limited capability of correcting higher-order aberrations, including coma and spherical aberrations.

Due to these drawbacks, we propose a computational solution that modifies the optics of electronic displays for correcting refractive visual aberrations. Our solution is safe with no direct contact with the eye. It improves the image pre-distortion architecture proposed by Huang et al. [17] that sends a sharp image without distortion to the focal range of the viewer by displaying a light field in front. The light field display and pre-distortion algorithm are constructed with a microlens array to eliminate the brightness loss and diffraction of the pinhole aperture array in prior work. The chromatic artifacts are erased by multi-sampling within the primary light emitting diodes in the pixels of the display panel. A preprocessing image quality enhancement method is proposed and significantly improves the perceptual experience according to the HDR-VDP2 image quality evaluation. Finally, we implement the application of the light field vision correcting method to a low-cost virtual reality head-mounted display using Google Cardboard.

To my parents.

Contents

Contents **ii**

List of Figures **iv**

List of Tables **vi**

1 Introduction **1**
1.1 Background 1
1.2 Vision Correcting Display Technology 3

2 Related Works **4**

3 Human Visual Aberrations **6**
3.1 Human Visual System 6
3.2 Image Blur as a Function of Defocus and Pupil Size 6
3.3 Types of Refractive Aberrations 7
3.4 Wavefront Aberrometer Measurement 10

4 Light Field Display **13**
4.1 The Plenoptic Function 13
4.2 Pinhole and Microlens Array 13
4.3 Limitation Analysis 14

5 Microlens Array Based Image Prefiltering **16**
5.1 Light Field Prefiltering 16
5.2 Parameter Setup 17
5.3 RGB Sub-Pixel Arrangement 18

6 Light Field Image Perception Simulation and Evaluation **21**
6.1 Microlens Array Simulation 21
6.2 Image Quality Evaluation Metrics 22
6.3 Image Quality Enhancement 23

7 Optical Analysis and Design of Hardware Prototype **24**
7.1 Pinhole Array Mask Design 24
7.2 Microlens Array Design Optimization 24

8 Application in Virtual Reality Head-mounted Display **27**
8.1 Background 27
8.2 Virtual Reality Stereoscopic Display 28
8.3 Single Lens Model Approximation 28
8.4 Experiment Evaluation 30

9 Conclusion and future work **34**
9.1 Microlens Array Vision Correcting 34
9.2 Vision Correcting in VR Head-Mounted Display 35

Bibliography **36**

List of Figures

3.1 Geometrical model of defocus in a myopic eye. 7
3.2 Decrease in amplitude of accommodation with age. [38] 9
3.3 Imaging of lens with astigmatism [17]. 9
3.4 Zernike polynomials up to the 6th order [21]. 11
3.5 wavefront aberrometer. 11
3.6 Higher-order wavefront aberration (top row) and point spread function (bottom row) analyzed from three sets of Zernike polynomial functions measured with Shack-Hartmann wavefront aberrometer over a 5 mm pupil. 12

4.1 Demonstration of single lens unit of the microlens array light field display. . . . 14

5.1 Color gamut measurement of iPad 2 and newest iPad of 2012 (iPad 4) with Retina display [48]. 19
5.2 The sub-pixel light emitting diode arrangements in commercial display. 20

6.1 *Backward* ray tracing of microlens array in comparison to pinhole array display. 22
6.2 Simulation, physical capture, and HDR-VDP2 evaluation of the image pre-sharpen algorithm. 23

7.1 Trade-off between angular resolution and spot size to calculate the optimal pinhole size that yields best possible angular resolution. 25
7.2 Analysis of microlens design by Zemax simulation. Left column: Point spread diagram of microlens with light from center pixel (top) and corner pixel(bottom); Middle column: MTF of microlens with light from center pixel (top) and corner pixel(bottom); Right column: field curvature of microlens. 26

8.1 Stereoscopic VR near-eye display with normal-sighted eyes (left) and myopic eyes (right). Two yellow marks representing the same point in 3D object are converged to sharp points on retina. 29
8.2 Schematics for single lens model approximation (left) and light field optical setup (right) using microlens array and pinhole aperture array 30

8.3 Experiment prototype with a pinhole array held by a 6 mm acrylic transparent plate on top of the display of mobile device, is placed inside the Google Cardboard to form a VR display system with visual correction. 31
8.4 Experiment results comparing visually corrected image (d) with blurry image observed with near-sighted eyes (c). Since the experiment is done with pinhole aperture array, the brightness loss may affect the visual comparison. Yet sharpness improvement is noticeable by comparing the fine detail such as the paws of the dinosaur fossil. 32
8.5 More experiment results evaluating the capability of vision correction of proposed method. Top row: desired sharp image pairs perceived on retina; Middle row: rendered inversely pre-blurred image pairs; Bottom row: corrected image pairs observed by DSLR through pinhole array. 33

List of Tables

7.1 Doublelet configuration. 25

8.1 Parameter Setup 31

Acknowledgments

I want to thank my advisor Prof. Brian A. Barsky for the guidance throughout the work during my Master's research as well as introducing me to the fun world of optometry and vision science. I want to thank Prof. Austin Roorda and Prof. Martin Banks for the courses I took in vision science, which provide great helps in my graduate research.

I thank Prof. Ren Ng and Prof. Laura Waller for being my committee members and giving me so many suggestions in the thesis writing. They also taught the first computational imaging class when I came to Berkeley. The BCCI talks every week are inspiring and benefit me a lot in research.

I would also like to thank my mentor Dr. Ward Lopes and Dr. Fu-chung Huang during my internship at Nvidia, as they are my role models of being a researcher.

The two-year stay in Visual Computing Lab won't be as happy as it is without the company of Xuaner, Biye, Qijing. Daniel offered great help during my thesis writing. I want to thank you all.

Chapter 1

Introduction

1.1 Background

According to the global estimates of visual impairment 2010 [35] from the most recent data by Word Health Organization (WHO), visual impairment in 2010 is a major global health issue among the WHO regions. Surveys from 39 countries show the number of people of all ages visually impaired is estimated to be 285 million, of whom people of age 50 and older represent 65% of visually impaired.

The principal causes of visual impairment are uncorrected refractive errors that take up 43% of all global causes of visual impairment according to the definition of presenting vision in the International Classification of Diseases version 10. In adults, the estimated pool prevalence of myopia, hyperopia, and astigmatism was 26.5%, 30.9%, and 40.4% respectively [15]. These uncorrected refractive errors are shown to be responsible for visual impairment in 101.2 million people and blindness in 6.8 million people in 2010 [31]. Myopia that shortens the focusing range to a nearer region is estimated with growth from 22.9% of the world population in 2000 to 49.8% by 2050 [16]. Such prevalences of myopic population is even higher in the US [44] and some Asia countries [45]. Hyperopia, the refractive vision aberrations that only allows the observer focus at a farther range of objects, is studied by Castagno et al. [5] who concluded that age has an inverse association with hyperopia among children.

Presbyopia, the age-related loss of accommodative amplitude, is experienced by most people of age 50 or older [25]. Nearly 1.7 billion people worldwide suffer vision issues due to presbyopia in 2012, and it is estimated to grow to 2.1 billion by the year 2020 [39].

Aside from lower-order aberrations caused myopia, hyperopia, presbyopia, and astigmatism, there exist higher order aberrations such as coma, spherical aberration, and trefoil that can cause difficulty seeing at glare, halos or night. The fact that no eye is perfect implies that all eye has a non-zero degree of certain higher order aberrations [42]. Attention has been

focused on higher order aberrations ever since the invention of wavefront technology that helps diagnose them, and it draws even more research interests of vision scientists recently because they are identified as some of the severe side effects of refractive surgery.

Options of Vision Correcting Treatment

The most commonly used tools to correct lower order aberrations are eyeglasses. The concave lenses for myopia and astigmatism, convex lenses for hyperopia, and bifocal lenses for presbyopia predominant the market of daily based refractive error vision correcting equipment for hundreds of years. However, wearing eyeglasses leads to unsatisfying visual experiences more and more recently with the popularization of modern visual entertainment such as 3D movie and virtual reality. Senior people with presbyopia are forced to put on glasses whenever they want to focus on a nearer object and take them off when looking back to a farther object, which is neither convenient nor efficient.

The first plastic contact lens was produced in 1949, and years after that did soft contact lens become an option for long-wearing vision correcting method that fits the anterior of the eye and compensates the refractive error. The progress of contact lens manufacturing technologies makes it accepted by a more substantial population now and able to be used for cosmetic purposes, although a considerable number of people still feel uncomfortable when wearing contact lens for an extended period. Besides, it should not be neglected that people with severe astigmatism are offered with significantly less amount of choices regarding of contact lenses.

Refractive surgery, on the other hand, is proposed to modify the optical power of the eye by directly modify the shape of the cornea. It has been around a few decades since the first generation of patient underwent refractive surgery in late 20 century. Despite continued improvement in technologies and increased experience of surgeons, complications occur at a low incidence, which can be related to inadequate preoperative screening, intraoperative factors, postoperative problems or refractive issues [11, 27, 40]. A survey [24] among 161 eyes in 101 patients with ocular complaints showed that the most common complaints were overcorrection (30.4%), irregular astigmatism (29.8%), dry eyes (29.8%), glare (26.1%), difficulty with night driving (16.7%), and corneal haze (16.7%).

For higher-order aberrations, methods for correcting them are actively studied at present. Adaptive optics including new kinds of high-definition eyeglasses, contact lenses and refractive surgery are customized to adjust the shape of the corneal surface. But still, awkward wearing experiences caused by glasses, discomfort of contact lenses and side effect risk of refractive surgery prevent people from keeping relying on them.

1.2 Vision Correcting Display Technology

Other than any of the above methods, an alternative option for correcting refractive visual aberrations is proposed in the previous work done by Fu-Chung et al. [17]. Opposite from altering the refractive power of the eye, a computational display is produced to "*present the pre-distorted content according to the viewer's prescription, such that a sharp image is formed on the retina*.", Which only includes software computation and optical hardware component - a pinhole array mask - attached to the display device. Thus the vision correcting display has no direct contact to the observer and will not cause any discomfort of the eyes. An integrated framework called light field prefiltering is prototyped to provide both high resolution and high image contrast and is theoretically proven to be capable of correcting both lower and higher order aberrations.

In this work, we improve upon the idea of light field vision correcting display and achieve an even better perceptual experience while significantly speeding up the prefiltering algorithm. Microlens array is proposed as an alternative to the conventional pinhole array to achieve better brightness with accurate simulation and optimized design. In addition to the original scenario of applying to normal viewing distance for daily reading, we further test this idea to a near-field display - VR head-mounted display (HMD), aiming at increasing the immersive experience of virtual reality for people who feel cumbersome wearing double glasses.

Chapter 2

Related Works

Glasses-free 3D Display

Traditional non-digital technologies of the glasses-free 3D display include integral photography, parallax panoramagrams, and holography. In additions to that, digital techniques were introduced by Lippmann [28] and Ives [23] by placing an array of lenticular lens or parallax barrier over a high-resolution display. Matusik [30] implemented a glass-free 3D TV system with a real-time acquisition, transmission, and presentation. Fuchs [10] presented designs of multi-dimensional displays which passively react to the light of the environment behind by physically implementing a reflectance field and generating different light fields depending on the incident illumination. Huang et al. [19] proposed inverse prefiltering for high resolution emerging multilayer displays that mitigate contrast loss and eliminating ringing artifacts observed with single-layer prefiltering.

Light Field

The light field has undergone great interest in research since late 20 century. Adelson and Bergen [2] introduced the plenoptic function to define the total geometric distribution of light over the 5D space. Levoy et al. [26] and Gortler et al. [14] reduce the 5D plenoptic function to a 4D light field and show that extracting appropriate 2D slices from the 4D light field can produce novel views of the scene. Adelson and Wang [1] introduced a plenoptic camera that can achieve "single lens stereo", which marked the start of modern research in light field imaging. Ng et al. [33] propose a plenoptic camera that can capture 4D light field in a single photographic exposure and execute digital refocusing to the captured image [32].

Near-Eye Light Field Display

Lanman et al. [20] proposed a near-eye light field display using microlens array that is capable of presenting sharp images depicted by out-of-focus element. However, the size of eye boxes is too narrow to yield an immersive experience. Aksit et al. [3] builds a wide field

of view (FoV) near-eye head-mounted display (HMD) for virtual reality applications that adopt a pinhole aperture mask and a display screen.

Vision Correcting Display

Fresnel holograms serve as a potent method due to its unlimited degrees of freedom in optical correction. However, the aberration correction capability of computer-generated holography (CGH) is limited to the angular steering capability of the spatial light modulator (SLM). Similarly, the computational vision-correcting display has the limitation of trading off angle and spatial resolution and has been studied over the years. Pamplona et al. [34] used light field displays to generate a virtual image within the observer's focal range with sufficiently high angular resolution yet low spatial resolution. Hence, the viewer sees a corrected image but at a significantly lower resolution than that of the screen. Huang et al. [19] proposed a multilayer device with high spatial resolution but reduced contrast. A year after which, Huang et al. [18] introduced a pinhole aperture array based light field display that decreased the demands of angular resolution and thus achieved significantly higher spatial resolution. However, the brightness loss due to the pinhole array mask remains unsolved.

In this work, we propose a microlens array based light field display to increase the brightness while keep a high contrast and spatial resolution to provide a computational solution to correct refractive visual aberrations. Furthermore, we applied the proposed technology to virtual reality display to achieve an immersive experience with a wide field of view.

Chapter 3

Human Visual Aberrations

3.1 Human Visual System

Eyes are the only organs that can visually percept the world. The eyes detect light and convert it into neural signals and transmit to the visual cortex in the brain.
Cornea acts as the most important role when converging the light rays from real word into the eye. It is the front surface of human eyes that transmits light from back of the cornea to the aqueous humor with a total refractive power of around +43 diopters.
Pupil governs the image quality, depth of focus, field of view and keeps the vision system from overexposure or underexposure. The size of pupil varies among individuals and time since it is affected by many factors including light conditions, attention, emotion, age, etc.
Crystalline Lens has non-uniformly distributed refractive indexes and bends the light as it passes through to achieve a total power of around +21 diopters. In an **accommodated** eye, the ciliary muscle contraction causes constriction of the pupil and relaxes the zonular tension on the equator of the crystalline lens so as to increase the surface curvature and achieve a higher power of refraction around +32 diopters.
Retina is the sensor of the eye consisting of several layers of interconnected neurons. The neural cells that are sensitive to light are called the photoreceptor cells, and two of the most critical types of retinal photoreceptor cells that contribute to vision are rods and cones. **Rods** are sensitive to luminance and dominant in dim light, while the three types of **cones** response respectively to the chromaticity of light.

3.2 Image Blur as a Function of Defocus and Pupil Size

When modeling the human eye vision system, the cornea, crystalline lens and pupil altogether can be simplified as a single thin lens with a constant refractive index. Given the internal diameter d_e of the eye to be the distance between sensor plane and the lens, and the equivalent

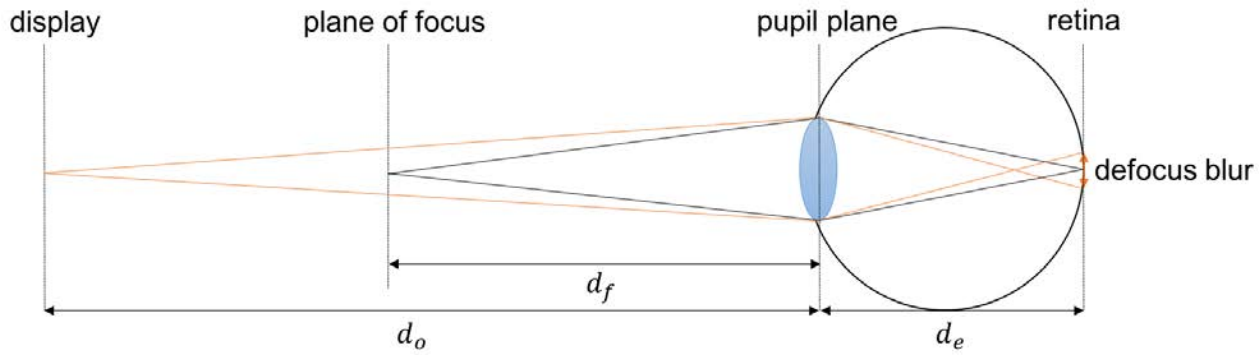

Figure 3.1: Geometrical model of defocus in a myopic eye.

focal length f of the synthesized lens, the distance d_f to the plane of focus can be determined using the thin lens equation:

$$\frac{1}{d_f} + \frac{1}{d_e} = \frac{1}{f} \tag{3.1}$$

An eye with normal vision adjusts the optical power of its crystalline lens as an accommodation to focus from infinitely far away to a position in 125mm ($d_f \in [\infty, 125]$). On the other hand, when the object is placed far from a myopic eye at a distance d_o, as is depicted in Fig. 3.1. Light rays from each point source on the object are brought into a focused point in front of the retina, and cause a circular blur on the retina. The diameter of blurring circle is calculated using similar triangle as $r_b = a(d_e/d_f - d_e/d_o)$, where pupil diameter a is in direct proportion to the retinal blurriness.

3.3 Types of Refractive Aberrations

The refractive errors of the eye can be divided into two categories - lower-order aberrations and higher-order aberrations. A large number of populations commonly experience lower-order aberrations including myopia, hyperopia, presbyopia, and astigmatism. Higher-order aberrations are proven to exist in every visual system yet only severe aberrations require correction by optical or medical technologies.

Myopia and Hyperopia

On average, a relaxed, healthy eye has a focusing power of around 60 diopters. The focal length of the eye is derived by $f = 1000/60 \approx 16.67$ mm. An object placed in infinity can be converged onto the retina (the focal plane of the lens). Therefore the equivalent distance in the air from the lens to the retinal plane of average human eyes is $d_e = 17$ mm. Notice that the actual length of the human eyeball along the optical axis is around 22.5 mm. However,

since the internal liquid media of human eyeball has a refractive index of $n = 1.33$, the equivalent length in the air is $22.5/1.33 \approx 17$ mm.

While focusing at a closer distance, the ciliary muscle relaxes and allow the crystalline lens to provide approximately 8 additional diopters, and such a process is called accommodation. Thus the eye lens has a focal length $f = 1000/68 = 14.7$ mm, and by applying into the thin lens equation, the nearest plane of focus is around $d_f = (f - d_e)/f/d_e \approx 125$ mm.

A myopic eye has more than 60 diopters converging power. An object from infinity is focused in front of the retinal plane and causes circular shaped blurring. The range of distance that can be perceived in focus is drawn close to the eye. A +5D myopic eye sees sharply from approximately 162 mm to 70 mm. A hyperopic eye, on the other hand, has its focal range farther from the eye since closer objects are focused behind the retina and end up with blurriness. A -5D hyperopic eye, for example, can perceive sharp images of objects placed from infinity to 239 mm.

Presbyopia

Even though presbyopia describes a similar scene of having trouble to see a closer object, different from hyperopia, it is caused by losing the capability of accommodation of the crystalline lens. The Elasticity of human crystalline lens decreasing [9] and the lens growth [37] with aging are shown to be the primary attributes of presbyopic eyes. Studies on optical changes in the human crystalline lens with age [12] shows that younger lenses can undergo significant changes in focal length with stretching, whereas lenses of people after age 60 show no changes in focal length with stretching produced by zonular tension. The additional optical power by accommodation decreases as the age growth by roughly one diopter every 3 to 4 years and becomes approximately 0 diopters after age 60 as is shown in Fig. 3.2. The presbyopic eye can be modeled with a fixed focal length lens that can only focus at a single distance. The focal length of the synthesized lens of the eye is affected by the degree of myopia or hyperopia of the eye, which is caused by a combination of the shape changes of the cornea, crystalline lens as well as eyeball.

Astigmatism

Irregular curvature of the underlying mechanism within the eye including cornea and crystalline lens can cause astigmatism. It is a type of unevenly distributed refractive aberrations that cause blurred vision at all distance as the two axes have different focusing power as is shown in Fig. 3.3. Therefore the blurred image of a point light source is an elliptical shape.

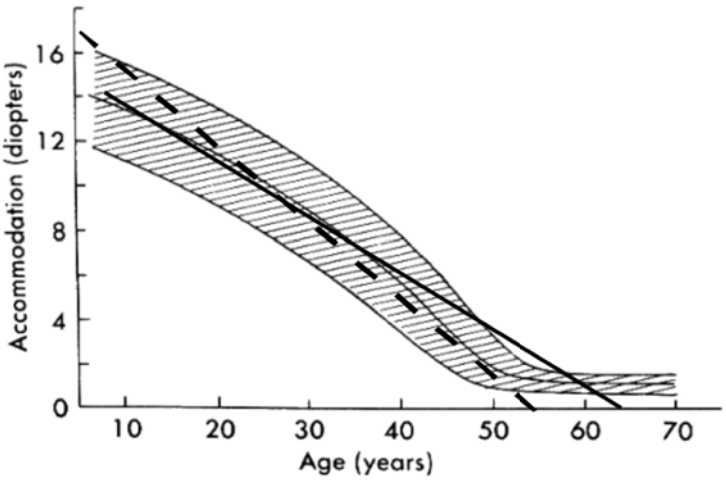

Figure 3.2: Decrease in amplitude of accommodation with age. [38]

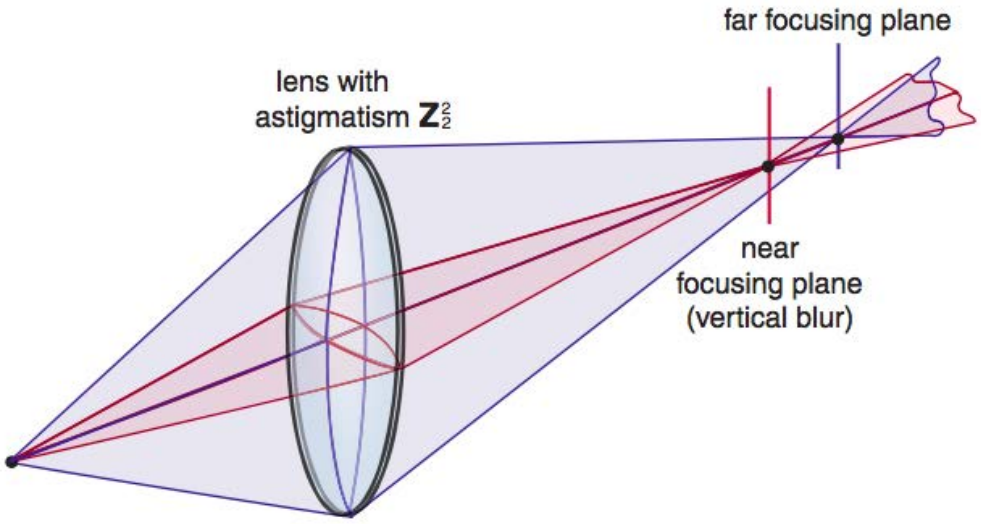

Figure 3.3: Imaging of lens with astigmatism [17].

Higher-Order Aberrations

The higher-order aberrations are due to the distortion of the wavefront of light caused by abnormal curvature of the cornea and crystalline lens. Significant higher order aberrations can also result from the scarring of the cornea surface or cataracts which have disabling impact on visual quality. The **Zernike polynomials** (Fig.3.4) named after optical physicist Frits Zernike [8] is proposed to be the best description of refractive aberrations of the cornea or lens, and the Zernike coefficients as the outputs of the wavefront aberrometer are now

widely used to detect any higher-order aberration.

3.4 Wavefront Aberrometer Measurement

The Shack-Hartmann wavefront aberrometer [36] is one of the most practical and robust techniques for measuring the ocular wave aberrations by taking the inverse process of tracing individual light rays from the outside world into an eye. A narrow beam of laser light is sent into the eye from the photodiode light source, and the light rays reflected back out by the retina present as an aberrated beam that has irregular wavefront and contains the information of aberration introduced by the optics (crystalline lens and cornea) of the measured eye. In the experiment, the Shack-Hartmann wavefront aberrometer uses an 840nm super-luminescent diode as the light source. The deformed light rays are then imaged with an array of microlens that divides the wavefront into sections and focuses onto a set of points on a photon sensor (like a CCD camera) to record the local direction of the wavefront. The captured image is then analyzed to calculate and quantify the wavefront aberration that represents the defect ones eye possesses.

Each term of the Zernike polynomials stands for different wavefront aberration. Z_2^0 quantifies the degree of defocus as a symmetric blur. Z_2^{-2} and Z_2^2 represent astigmatism, where the two axes are 90 degrees to each other. Z_3^{-1} and Z_3^1 describes coma and Z_6^0 determines the spherical aberration. The most common aberrations people have and share the most significant diversities are in the 2nd order (Z_2^0,Z_2^{-2} and Z_2^2) including defocus and astigmatisms.

For higher-order aberrations, people rarely have severe problems, and therefore it is less frequent to see vast differences among individuals. Fig. 3.6 is computed based on the pre-analyzed Zernike polynomial of three people. The person of the first column wore glasses during the data acquisition, the person of the middle column had experienced laser refractive surgery, and the person of the third column wore soft contact lenses. In a word, all three sets of data demonstrate the existence of higher-order aberrations even after corrected by the three primary vision correcting method.

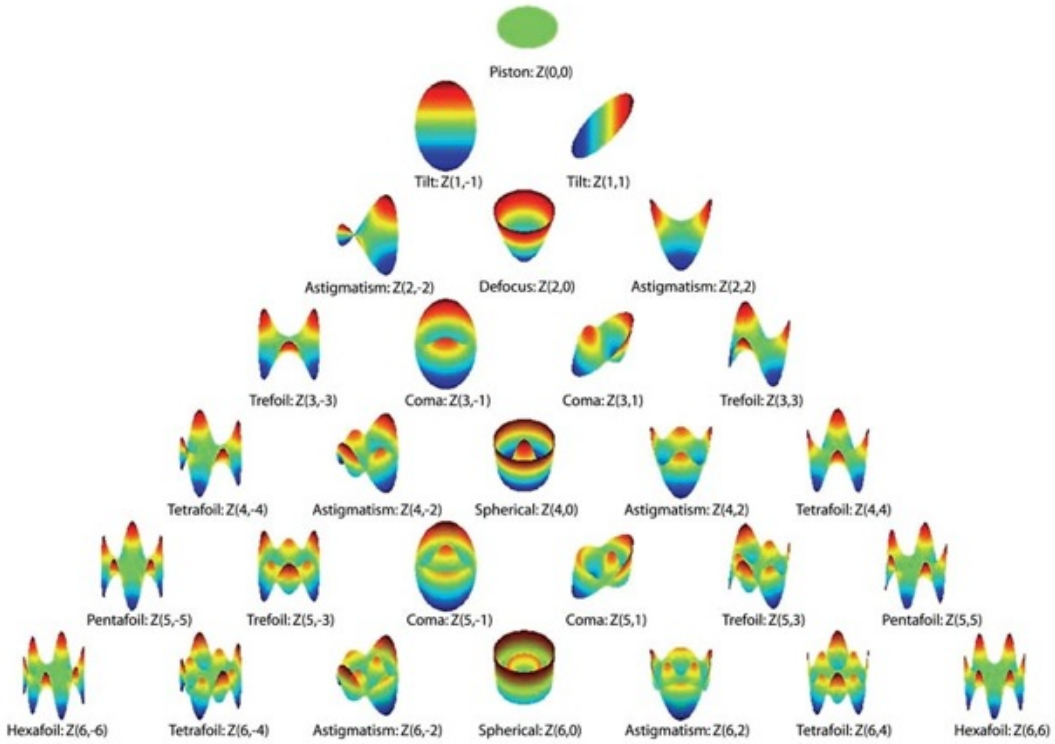

Figure 3.4: Zernike polynomials up to the 6th order [21].

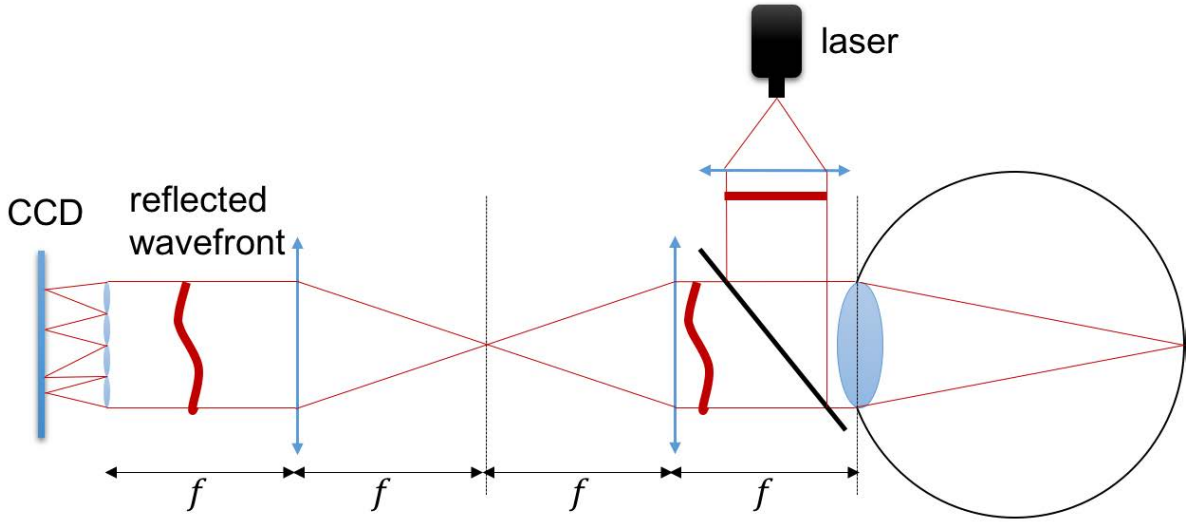

Figure 3.5: wavefront aberrometer.

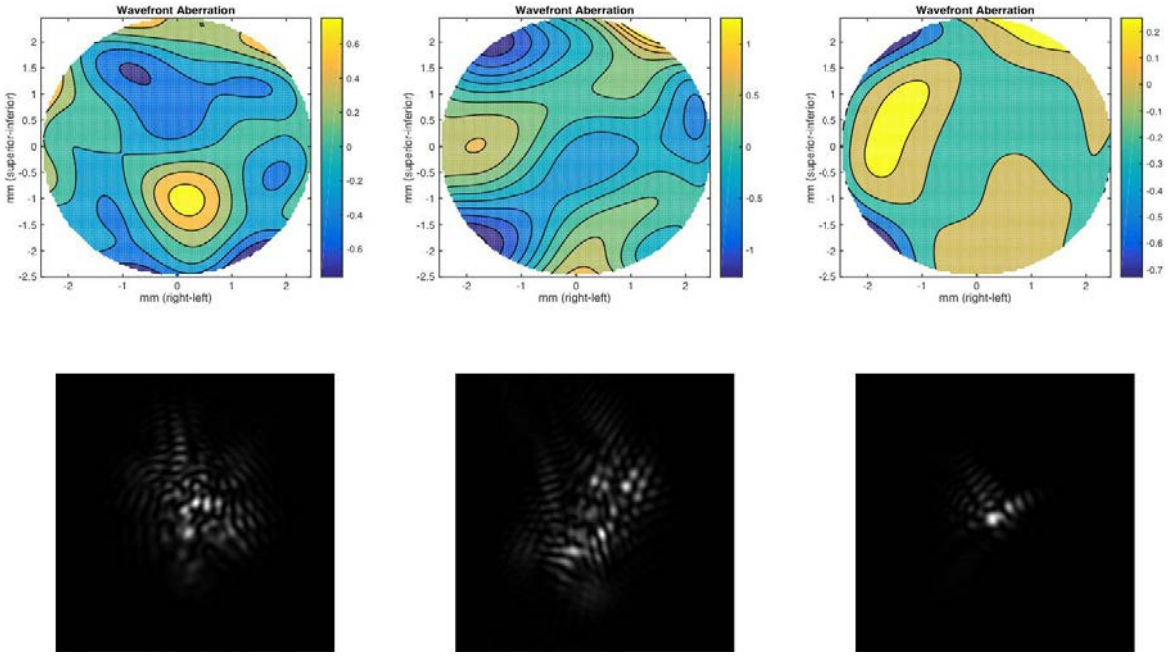

Figure 3.6: Higher-order wavefront aberration (top row) and point spread function (bottom row) analyzed from three sets of Zernike polynomial functions measured with Shack-Hartmann wavefront aberrometer over a 5 mm pupil.

Chapter 4

Light Field Display

Light field displays have been widely applied to achieve stereoscopic visual effect without requiring tracking or glasses. Viewers can receive different images in different viewing directions. Methods to construct such a 3D display includes non-digital technologies such as integral photography, parallax panoramagrams, and holography, as well as digital solutions placing an array of pinhole or microlens (lenslet) over a traditional display screen. In this chapter, we will introduce the principle of the light field and analyze the theoretical limitation of it.

4.1 The Plenoptic Function

In comparison to traditional displays that specify a 2D vector of point light source, the light field is a vector that describes light rays of certain direction through a point source in the space. The radiance along each ray is a 5D plenoptic function $L(x, y, z, \theta, \phi)$. Because any ray in space is parameterized by a point in 3D coordinates (x, y, z) emitting light in the direction (θ, ϕ). By restricting on the case that rays pass only through free-space so as the light is constant throughout the ray, one dimension of variation in plenoptic function is eliminated. Thus the light field, instead of 5D, is 4D in this work. On a light field display, each pixel emits different light rays in different directions aided by the parallax barrier or the microlens array. Therefore, the light field display acts like a virtual window to a 3D scene [43] that viewers are not required to wear glasses and can move around to any viewing location.

4.2 Pinhole and Microlens Array

A pinhole aperture array was proposed by Huang et al. [17] as the hardware prototype and is proven to yield a compelling power of vision correction. The pinhole size is set to be 75 microns to optimize light throughput and avoid diffraction, and the mask is mounted at an offset of 5.4 mm in front of an Apple iPod touch 4th generation display with a pixel pitch of

78 microns (326 PPI). The pinhole pitch is 5 times of pixel pitch of the screen.

The microlens array based light field display was introduced and implemented by Isaksen et al. [22]. They presented a passive autostereoscopic light field that can be viewed without head-mounted hardware by multiple viewers simultaneously. While the pinhole array is easy to design and manufacture, it is the primary cause of brightness loss and undesired Moiré artifact. Microlens array, on the other hand, is a transparent plate with an array of plano-convex lenses on one side that keeps the brightness of the conventional display and no more Moiré pattern due to the overlaid periodic pattern between pinhole array and display's internal structure of photodiode layout. Similar to the spatial ratio of one pinhole to 5-by-5 pixels, the microlens array is designed with the same ratio, namely one microlens is placed on above 5-by-5 pixel unit. Further detailed design and optimization of the microlens array will be discussed in chapter 7.

4.3 Limitation Analysis

One of the most significant drawbacks of light field display is the spatial resolution loss in the integrated display system. To analyze it as well as other property of light field display, we follow the relative two-plane parameterization introduced by Chai et al. [6]. The x-plane denotes the spatial coordinates, and the u-plane, 1-unit separated from the x-plane, indicates the angular directions as is depicted in Fig.4.1.

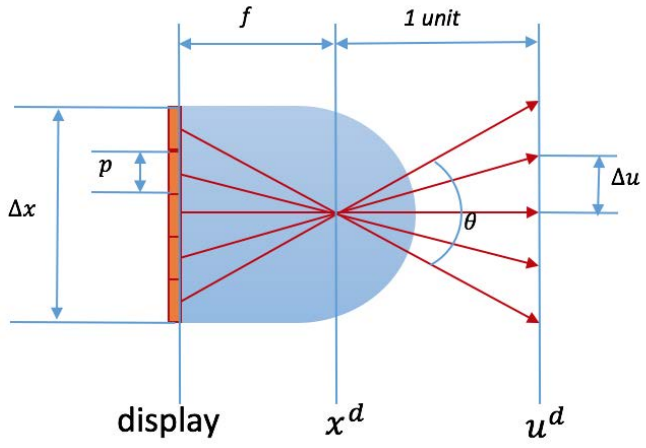

Figure 4.1: Demonstration of single lens unit of the microlens array light field display.

Spatial Resolution

In Fig. 4.1, Δx denotes the separation of adjacent microlens (spatial sampling rate) and p represents pixel pitch of traditional display. The spatial-angular trade-off ratio is therefore

$\Delta x/p$ and the light field display has $\Delta x/p$ views [17]. The construction of such a light field display uses a low spatial sampling rate to sample the original display panel. Thus the spatial resolution of light field display system is of pixel pitch Δx. According to the rule of Nyquist sampling [13], the maximum spatial frequency can be presented on such light field display is $1/2\Delta x$. In another word, any detail on the image finer than $2\Delta x$ causes aliasing in the perceived image. The loss of spatial resolution is unavoidable in the trade-off with the field of view. Thus high-resolution underlying display is essential for light field display. As observed by Pamplona et al. [34], light field displays present a compelling platform only once the resolution of display panel approaching 1900 PPI, which significantly exceed current commercial display panels.

Angular Resolution

The separation of two rays on the u-plane Δu denotes the angular sampling rate of the microlens array. The maximum angular frequency that can be presented on the display system is $1/2\Delta u$ according to the rule of Nyquist sampling. Any detail with an angular difference less than $2\Delta u$ viewed from a certain distance cannot be distinguished. To increase angular resolution, it requires high-resolution displays. Meanwhile, thicker microlens array panel (smaller f) and shorter viewing distance are preferred when perceiving images full of details.

Field of View

The field of view (FoV) θ is determined by the separation distance f between the optical center of microlens and the display panel as is shown in Fig. 4.1:

$$\theta = 2atan(\frac{\Delta x}{2f}) \tag{4.1}$$

Light field display of such a field of view is capable of emitting different $\Delta x/p$ rays/views across θ degree viewing zone even though undergoing a resolution loss at the ratio $\Delta x/p$.

Depth of Field

The depth of field (DoF) is an essential property of light field display as objects lying outside the range of DoF are blurred. It is crucial to analyze the depth of field of the light field display system since it depicts how far the image can be virtually displayed from the actual display panel while maintaining high enough image quality. The microlens array light field display has a depth of field defined by $\Delta x/\Delta u$. As the magnitude of defocus of the viewer results at a plane of focus farther than $\Delta x/\Delta u$ from the display enclosure, the image becomes blurred in a similar way to the out-of-focus effect, which shows a limited range of correcting power of the light field display.

Chapter 5

Microlens Array Based Image Prefiltering

As is discussed in previous chapters, the light field display is capable of synthesizing a semi-transparent virtual image layer at an arbitrary distance from the display surface to correct visual aberrations, where the optimal layer separation depends on the viewer's refractive error and distance to the display. It displays a pre-distored image on the display panel yet form an undistorted one on the retina. As the magnitude of aberration varies from person to person, the virtual layer may locate differently from the surface. However, the perceived image quality degrades if the virtual layer is too far from the display surface due to the depth of field limitation analysis.

Our idea is similar to the light field prefiltering method for automultiscopic displays proposed by Zwicker et al. [49], which is capable of uninhibited viewing from arbitrary positions and free from aliasing or artifact. Following the prior work by Huang et al. [17], we modify the conventional pinhole array based light field pre-distortion method for a better visual performance equipped with the microlens array. To explore the chance of future application in real-time video rendering, the microlens array prefiltering algorithm is built upon the *forward method* according to Zehao Wu [47], based on the "*light field based inverse prefiltering*" algorithm first introduced by Huang et al. [17].

5.1 Light Field Prefiltering

According to Huang et al. [17], the emitted light field is calculated by optimizing the objective function:

$$argmin_l \; ||i - Pl||^2 \tag{5.1}$$

Where i is the target retinal image, P is a projection matrix that stores the projective relationship of the locations of retinal sensor pixels and pixels on the conventional display

panel, and l is the inversely distorted image to be displayed on the screen. However, a non-negative linear solver is demanded to solve such a problem, which contributes a significant amount to the computational complexity of the original algorithm. It restricts the application of the vision correcting algorithm to video-based real-time rendering. So in our work, we simplified the projection model for significantly improved speed performance.

Model Simplification

To build the most thorough projection matrix P, tracing light rays between every retinal pixel and all possible aperture sample point is required. The time complexity of the algorithm is $\Theta(mn^2)$, where m is the number of samples on the pupil and n^2 is the number of pixels in target retinal image. To degrade the complexity, Wu [47] and Ding [7] simplified the model using the *forward method* and assume each screen pixel projects to only one retinal pixel through one pupil sample point and a single microlens. By removing the matrix computation, the total run-time of the prefiltering algorithm is significantly decreased to within 1 second with a complexity of $\Theta(n^2)$.

Moreover, the original programming language is chosen to be MATLAB which is beneficial regarding of its capacity of matrix computation. However, it is hard to optimize the time complexity in comparison to c++. The transportation from MATLAB to c++ was thus implemented for the *forward method* [47].

5.2 Parameter Setup

To deliver a desired 2D retinal image by presenting a 4D light field on a given viewing distance, the light field is pre-rendered based on the prescription of viewer's eye, viewing distance, and pupil size. Thus updating these parameters is required for frame by frame light field rendering.

Human Eye

The human eye has a flexible crystalline lens that changes its optical power according to chromatic retinal blur and the signal from the brain to focus at the desired distance. In this work, we assume that all the rest components, such as pupil size and the internal diameter of the eye, remain the same under any circumstances. When updating the eye parameter for a different viewer, we conclude that the modification is only required on d_f – the distance between the closest to display focal plane and the pupil, which can be calculated from the given prescription of the viewer's eyes. Alongside the internal diameter of average human eye $d_i = 17mm$ (equivalent eyeball length in the air), the eye's focal length f_e is derived by $f_e = d_i d_f/(d_i + d_f)$.

Camera

The fact that user test is hard to objectively evaluate the visual quality of the proposed light field display calls for camera test in the current stage. Different from human eye that has a fixed gap between lens and retina, the camera moves its lenses in order to focus at a different distance with a fixed focal length setting. Thus given a pair of focal length f_c and distance of focus point d_f, distance between equivalent optical center of lens set to the sensor d_i is derived by $d_i = f_c d_f/(d_f + f_c)$.

The aperture size a of a camera is controlled by the f_stop number setting where f_stop $= f_c/a$. To achieve an aperture size similar to human eye's average 6 mm, a 50 mm focal length lens needs to pair with a setting of f/8, 75 mm focal length with f/11 and any practical setting within the instrument.

5.3 RGB Sub-Pixel Arrangement

The wavelength-variant refractive index of the microlens array is one of the primary cause of chromatic artifact perceived in physical evaluation experiment, which calls for careful study in computing the projection relationship separately for each color channel. Rather than generating projection relationship uniformly for every pixel, it becomes essential to treat each predominant color sub-component (light emitting diode - LED) as a single point light source. And each ray of a single wavelength light can be traced according to its corresponding refractive index defined by the material of the microlens.

Color Vision and Electronic Display Anatomy

Photoreceptor cells responsible for color vision in the retina of mammalian eyes consist of three types of cones that are sensitive to short, medium and long wavelength spectra respectively. Studied from this fact, vision scientists proposed the trichromatic color matching functions [46] that indicates any monochromatic light (single wavelength light) of equal radiance matches a set of red, green, and blue primaries:

$$\bar{r}(\lambda)R + \bar{g}(\lambda)G + \bar{b}(\lambda)B \approx \lambda \tag{5.2}$$

$$\begin{aligned} R &= 700nm; 72.1W \cdot sr^{-1} \cdot m^{-2} \\ G &= 546.1nm; 1.4W \cdot sr^{-1} \cdot m^{-2} \\ B &= 435.8nm; 1\ W \cdot sr^{-1} \cdot m^{-2} \end{aligned} \tag{5.3}$$

The CIE 1931 standard color space that became the "industry standard" is a linear transform of the primaries on above:

$$\begin{pmatrix} \bar{x}(\lambda) \\ \bar{y}(\lambda) \\ \bar{z}(\lambda) \end{pmatrix} = \begin{pmatrix} 2.7689 & 1.7517 & 1.1302 \\ 1.0000 & 4.5907 & 0.0601 \\ 0 & 0.0565 & 5.5943 \end{pmatrix} \begin{pmatrix} \bar{r}(\lambda) \\ \bar{g}(\lambda) \\ \bar{b}(\lambda) \end{pmatrix} \tag{5.4}$$

$$\begin{aligned} X &= \int P(\lambda)\bar{x}(\lambda)\mathrm{d}\lambda \\ Y &= \int P(\lambda)\bar{y}(\lambda)\mathrm{d}\lambda \\ Z &= \int P(\lambda)\bar{z}(\lambda)\mathrm{d}\lambda \end{aligned} \tag{5.5}$$

$$\begin{aligned} x &= \frac{X}{X+Y+Z} \\ y &= \frac{Y}{X+Y+Z} \\ Y &= luminance \end{aligned} \tag{5.6}$$

Where the CIE tristimulus (X, Y, Z) and chromaticity coordinates (x, y, Y) are the most commonly used descriptors to specify a light with spectrum $P(\lambda)$. Modern electronic visual display, informally a screen, present visual information with pixels consisting of three types of light emitting diode (LED) of three primary colors - red, green and blue. An example of dominant colors of the iPad 2 and iPad 4 is shown in Fig. 5.1.

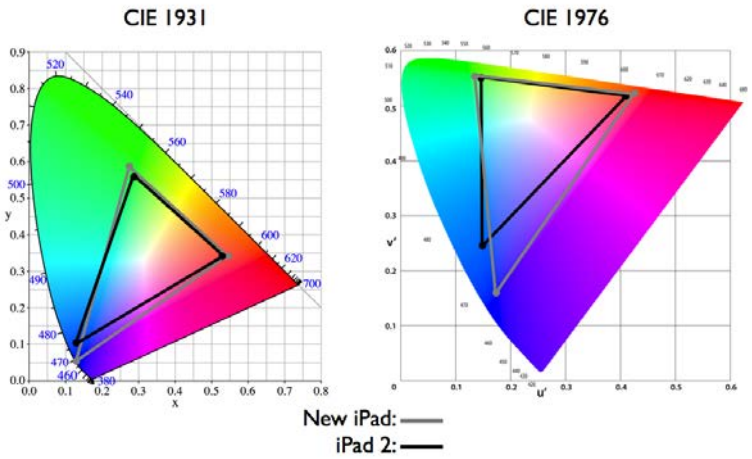

Figure 5.1: Color gamut measurement of iPad 2 and newest iPad of 2012 (iPad 4) with Retina display [48].

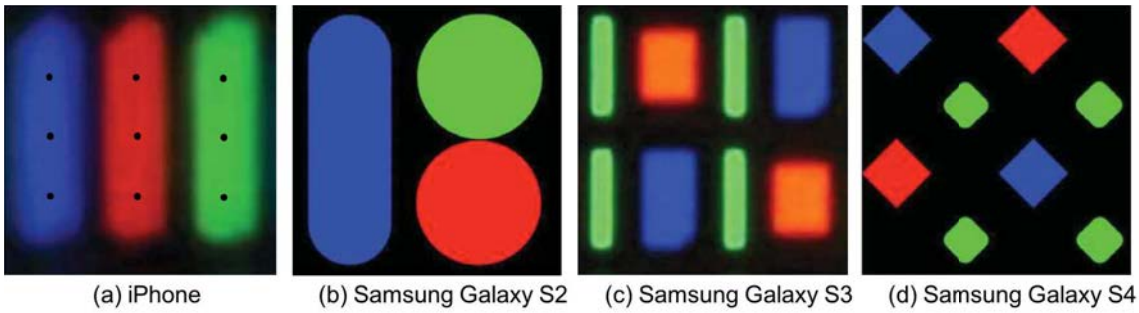

Figure 5.2: The sub-pixel light emitting diode arrangements in commercial display.

Sub-pixel sampling and Multi-sub sampling

In the light field prefiltering algorithm introduced by Huang et al. [17] and improved by Wu [47], each pixel on the display panel was treated as a point light source, and light rays were traced from the center of the square pixel. The microlenses are designed in a way that their focal plane overlays the display panel, so they convert the diverging light beam from one pixel to a parallel beam of light. Thus the total amount of possible directions of light rays from one pixel is restricted to a finite number. Because human eye has relatively small pupil size, it is unavoidable that none of the light beams from one pixel can pass through and then the pixel is missed. In a result, the prefiltering image contains a considerable amount of black region.

To avoid such instance, we propose a sub-pixel sampling method by taking each primary light emitting diode in the screen as an actual point light source. Which significantly increased the possibility of light rays passing into the pupil while constructing projection relationship. For the display of the iPhone 6 in Fig. 5.2 (a), we sample the center of each sub-pixel as the position to trace a ray from which.

However, cases still exist that within one pixel not all three of the primary LEDs can be projected to the retina. Such a pixel is then assigned with the intensity of only one or two color channel instead of full-color space and contributes to the undesired chromatic artifact of the vision correcting light field display. Solution to such a problem was then implemented by making additional sampling to each sub-pixel and seeking chances of hitting the retina. Fig.5.2 (a) shows an example of 9-point sampling on each pixel.

One thing worth noticing is that, in addition to the different choices of color gamut among the mainstream display in the market, they share different structure of LED layouts. Thus different projection relationship constructions are demanded for different displaying devices. The iPhone 6 has each pixel composed of rectangular shaped blue, green and red LEDs as is depicted in Fig. 5.2 (a). The Samsung Galaxy series, on the other hand, make changes between each version of the display as is shown in the rest of Fig. 5.2.

Chapter 6

Light Field Image Perception Simulation and Evaluation

The physical result capturing from the pinhole array based light field display prototype is crucial and well tested in this work. Photographs are obtained with a DSLR camera simulating a human eye with defocus refractive aberration. Although this experiment is essential in demonstrating the vision correcting capability of the proposed light field display, it is hard to objectively evaluate the image quality performance since the capturing process is susceptible to the environment. The alignment of the units on the pinhole array and pixels on display panel is one of the factors that affect the perceptual result the most. As a result, software simulation of the light field image perception process is demanded for the evaluation of the light prefiltering algorithm.

6.1 Microlens Array Simulation

As is introduced earlier, the light field prefiltering algorithm uses the "*forward method*" for complexity degradation yet sacrifices an information loss. The simulation of light field image perception process is implemented with the "*backward method*" for protection of image quality by reserving a sufficient amount of contributory rays for each retinal pixel.

Fig. 6.1 depicts the intrinsic ray tracing model in the simulation algorithm for microlens array in comparison with pinhole array. Random sample points within the pupil together with each retinal pixel forms all possible light rays contributing their intensity to that retinal photoreceptor. During the process of "*backward method*", these rays are bent according to the prescription of the eye and hit the microlens array or pinhole array. While the pinhole array blocks most of the rays and allows only part of them to pass through, the microlens array keeps all of the light rays and refract them to the display panel. The projection relationship is generated to convert the displayed prefiltering image to the simulated perceptual image as shown in the second column in Fig. 6.2.

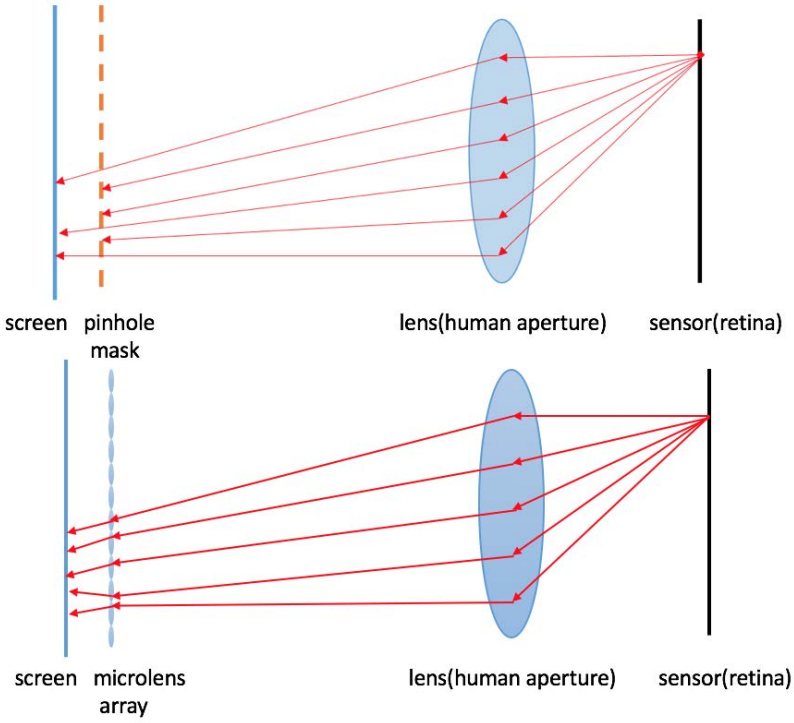

Figure 6.1: *Backward* ray tracing of microlens array in comparison to pinhole array display.

6.2 Image Quality Evaluation Metrics

Root Mean Square Error

The root mean squared error (RMSE) is one of the full-reference image quality evaluation metrics that quantifies the difference between the test image and its reference image. It computes the cumulated pixel-wise differences between test image I_t and reference image I_r in the following way:

$$RMSE = \sqrt{\sum_{x}\sum_{y}\sum_{c\in\{r,g,b\}}(I_t(x,y,c) - I_r(x,y,c))^2} \tag{6.1}$$

RMSE is good enough to show an overall score that describes the similarity of simulation result and desired retinal image. However, it is not adequate in telling how the information loss spatially allocates in the image.

HDR-VDP2 Perceptual Evaluation Metric

The HDR-VDP2 [29] is a perception-based full-reference image evaluation metric that assesses both contrast and sharpness by predicting a visibility map on the probability of how

discernible the differences are to an average observer. We take the output of HDR-VDP2 - a probability map of perceptual detection of differences between the simulation results and the desired retinal images, as shown in the last column of Fig. 6.2. It is noticeable that visible differences occur mostly around the margin of the image, the edge of objects, and fine details.

6.3 Image Quality Enhancement

The image quality degradation resulting from the microlens array light field display is unavoidable regarding resolution and contrast loss. The HDR-VDP2 evaluation results additionally show that such quality loss happens mostly on the high-frequency components of an image. Therefore we propose an image quality enhancement method in addition to the light field prefiltering algorithm.

The simplified *forward* image pre-distortion algorithm approximates a linear transform of the 2D image, which implies that the sequence of convolution does not affect the outcome. To improve the sharpness of the perceived image, we can pre-sharpen the input image before being fed into the prefiltering process. Here we use Wiener filter to sharpen the desired retinal image. In Fig. 6.2, the top row demonstrates the simulation, camera capturing result and the quality evaluation result of the light field pre-distortion algorithm, while the bottom row shows the corresponding result of a pre-sharpened target image (lower left image). Both simulation and physical test show impressive image quality improvement in the pre-sharpened results comparing the original algorithm.

Figure 6.2: Simulation, physical capture, and HDR-VDP2 evaluation of the image pre-sharpen algorithm.

Chapter 7

Optical Analysis and Design of Hardware Prototype

As is discussed in previous sections, the light field display is commonly built with an array of small magnifying lenses – a microlens array or an array of small apertures – pinhole array. Both of them share the same capability of controlling light rays to the desired directions. The pinhole array is considered to be a low-cost option to test the algorithm. However, the brightness loss and Moiré artifacts caused by pinhole mask suggest a preference for the microlens array.

7.1 Pinhole Array Mask Design

The optimal size of the pinhole is the result of a trade-off between angular resolution and spot size on the cornea. The pinhole aperture size p is positively correlated with the angular resolution of the light field display, which can be calculated using Rayleigh resolution formula $\theta \approx \lambda/p$. However, a growing pinhole size leads to an increasing spot size illuminated on the cornea and causes extra blurriness to the perceived image ($\theta \approx p/(2t)$). These two constraints meet at the optimal pinhole size which is given as $p = \sqrt{2\lambda t}$. The best pinhole size p can be chosen according to the interval t between the display screen and optical layer of the pinhole array, to achieve the best possible angular resolution.

7.2 Microlens Array Design Optimization

Lens Aberration

For an ideal lens, a point light source emitting light through will be focused to a single point at the plane of focus. While moving the point light source within a plane that is orthogonal to the optical axis, the focused point should remain in the same plane of focus. The relationship of the separation of object plane from lens d_o and the separation of focal plane

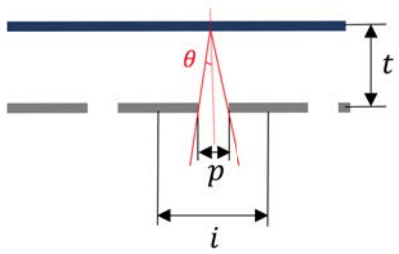

Figure 7.1: Trade-off between angular resolution and spot size to calculate the optimal pinhole size that yields best possible angular resolution.

	Radius of curvature	**Refractive index**	**Abbe number**
Concave lens	1.4805 mm	1.52	55
Convex lens	2.961 mm	1.65	45

Table 7.1: Doublelet configuration.

from lens d_i and the focal length of the lens f satisfy the thin lens equation $1/f = 1/d_o + 1/d_i$.

In actual, optical aberrations exist in any lens in a way such that light rays emitted from a point source do not converge to (or diverge from) a single point after transmission through the lens. This kind of unavoidable spherical aberrations is caused by the geometry property of the lens, and the smaller lens diameter leans toward more geometrical aberrations.

Zemax Microlens Optimization

In this work, we set the microlens to pixel correspondence ratio same as the pinhole array – 1 to 5-by-5 pixels and the separation from screen also 6 mm. Given the pixel pitch on the iPhone 6 screen is 0.078 mm, the size of a single microlens is 0.39 mm. Therefore, aberrations introduced by the optics of microlens array is not neglectable.

Aberrations of microlens array can be analyzed with the techniques of geometrical optics using Zemax. We simulate a plano-convex spherical lens with the radius of the convex surface being 2.961 mm, the center thickness being 0.5 mm, the diameter being 0.39 mm and material being PMMA.

The analysis of modulus transfer function as illustrated in Fig. 7.2 suggests that the proposed microlens array performs close to diffraction limit and the point spread spot diagram is within the region of tolerance. However, the field curvature analysis shows a difference in the plane of focus for RGB primary color component. To reduce such a chromatic aberration, the lens can be modified using doublet. The configuration of doublet according to Weiwen Di's simulation is shown in Table. 7.1.

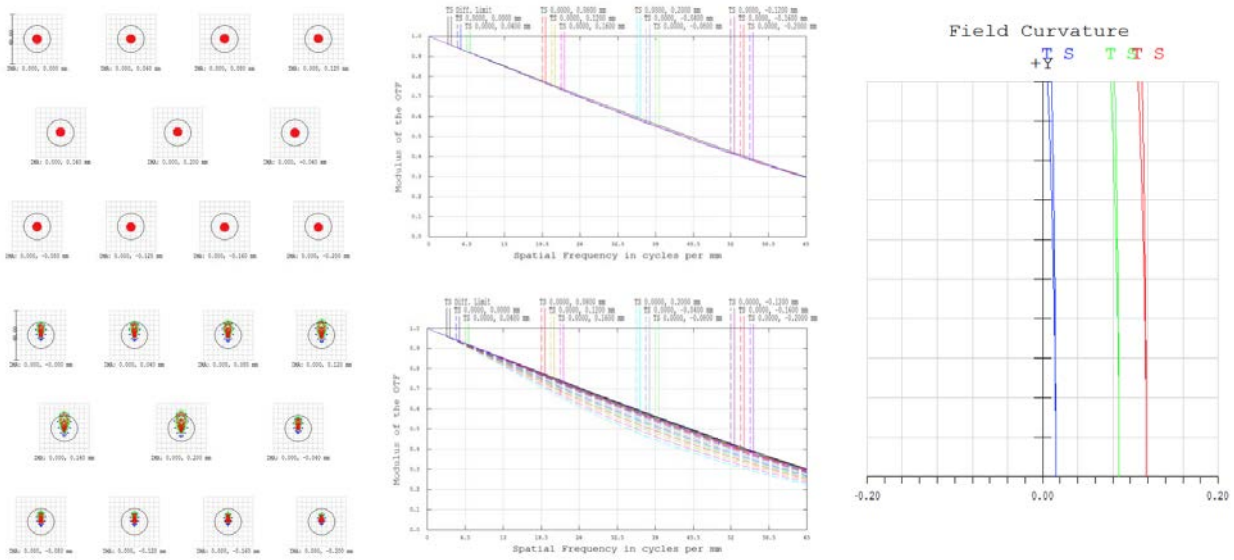

Figure 7.2: Analysis of microlens design by Zemax simulation. Left column: Point spread diagram of microlens with light from center pixel (top) and corner pixel(bottom); Middle column: MTF of microlens with light from center pixel (top) and corner pixel(bottom); Right column: field curvature of microlens.

Chapter 8

Application in Virtual Reality Head-mounted Display

The light field pre-distortion algorithm discussed in previous chapters is based on the assumption of perfect calibration of the relative position between the viewer's mono-eye and the display. However, in practice, it is unavoidable that the viewer can move his head to arbitrary distance and location. Therefore, rapid distance detection is required in real applications. Also, the prescriptions for the two eyes of a person are rarely the same, which requires the binocular architecture to send different images to each eye respectively. Sijia Teng et al. [41] proposed a real-time viewing distance measurement based on eye tracking techniques and built a binocular vision framework using parallax barriers.

The head-mounted displays, while keeping the relative position of the screen and the eyes, show great potential in application to the light field vision correcting architecture. In this chapter, we introduce the modeling of thin lens approximation in VR HMD and evaluate the result using a DSLR camera.

8.1 Background

Virtual reality head-mounted displays, after decades of development, have been widely used in entertainment, education, art, healthcare, military training, social science, and many other areas. Most modern consumer VR HMDs share major features including a high-resolution display, a pair of magnifying lenses or lens sets, gyroscopes or motion sensors for tracking head, hand and body positions, and a processor. By presenting two offset images separately to the left and the right eye, the viewer can combine the two 2D images in the brain and gain an illusion of 3D depth by binocular disparity. To bring the VR HMDs to a slim and compact form factor, the displays are usually placed 3 to 7 centimeters in front of the eyes, on where human eyes lose the capability to focus. A pair of lenses in between screen and eyes thus helps converge the angle of incoming light to focus on the retina.

Challenges in the design of near eye head-mounted displays include achieving high resolution, wide field of view (FoV), lightweight, reduced visual discomfort, and low cost. Lanman et al. [20] proposed a virtual reality near-eye head-mounted display (HMD) by placing microlens arrays in front of the microdisplays. Mobile phones, while providing substantial dimensions and high density around over 300 pixels per inch (PPI), are favored in low-cost HMD design. Kann et al. [4] proposed a slim near-eye HMD formed by a pinhole aperture array and a display screen to achieve a wider field of view compared to the conventional refractive element embedded VR HMD .

Low-cost VR HMDs such as Google Cardboard benefit large population for immersive VR experiences. However, they are manufactured only for normal-sighted users and do not contain adjustable architectures of the refractive lenses or the position of the mobile device, thus lack the capability of vision correction. In this work, we propose a computational display architecture utilizing pinhole aperture arrays to generate an image shown in the accommodation range of the viewer for correcting refractive visual aberrations. We build a low-cost prototype with the Google Cardboard and evaluate it with a DSLR camera.

8.2 Virtual Reality Stereoscopic Display

As demonstrated in Fig. 8.1, a point object has two corresponding points on the display for the left and right eyes, which can be seen as two point light sources, marked yellow in Fig.8.1 (left). Light rays from these two sources converge to two sharp points on the retina after being reflected by the magnifying lenses and the eyes. The brain then calculates the binocular disparity to extract the depth information of this virtual object point. This process can also be drawn as tracing back all the rays that come into the eyes and reaching the same virtual target point behind the display.

With the aid of magnifying lenses in VR HMDs, a normal-sighted eye can form a sharp representation of displayed images on the retina as is shown in Fig. 8.1 (left). However, same architecture does not work ideally for eyes with refractive visual aberrations such as myopia (Fig. 8.1 (right)). The most distant position that can be perceived sharply is in front of the actual display panel, and here we denote it as the plane of focus (green in Fig. 8.1 (right)).

8.3 Single Lens Model Approximation

The separations between the viewers' eyes and the lenses in VR HMDs are relatively close enough to be considered zero, and this assumption approximates the real case especially for near-sighted users as they would adjust the eye positions as much close as possible in order to

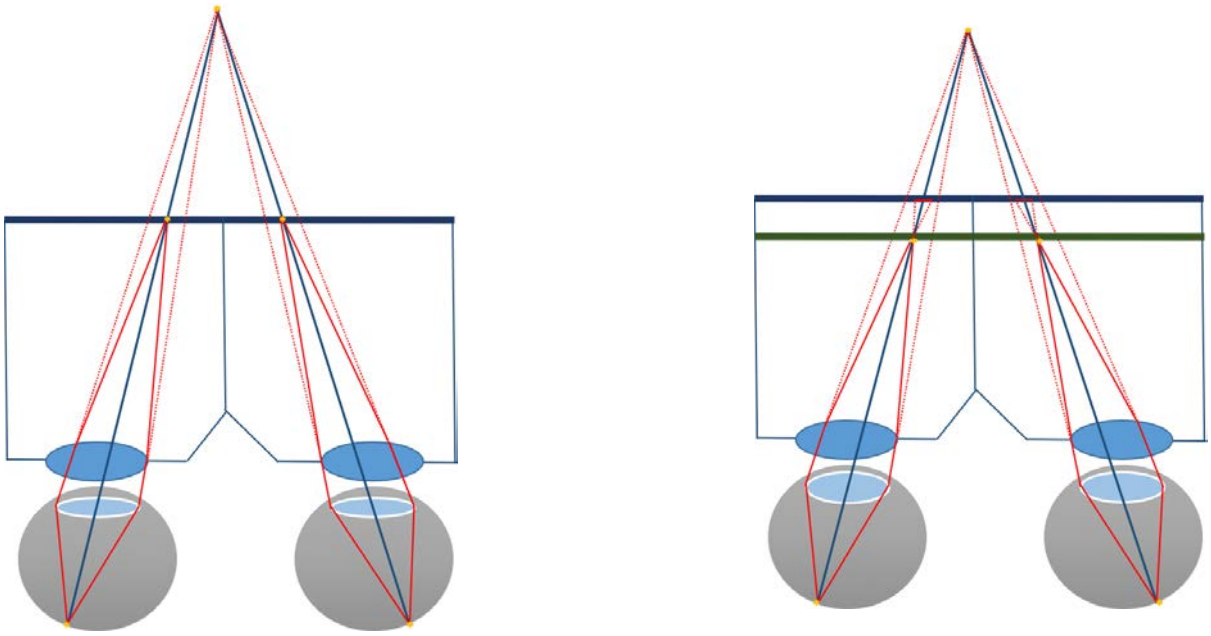

Figure 8.1: Stereoscopic VR near-eye display with normal-sighted eyes (left) and myopic eyes (right). Two yellow marks representing the same point in 3D object are converged to sharp points on retina.

see clearly. The total power of refraction of a two lens system can be equivalently produced by a single lens with focal length f:

$$f = \frac{f_1 f_2}{f_1 + f_2 - d} \tag{8.1}$$

Where f_1 and f_2 are the focal lengths of two lenses placed in separation d. In conditions that d is much smaller than one of the focal lengths, the last term in the denominator becomes negligible, and the equivalent diopter D, the reciprocal of the equivalent lens focal length given in meters ($D = 1/f$), is:

$$D = \frac{1}{f} \approx \frac{1}{f_1} + \frac{1}{f_2} = D_1 + D_2 \tag{8.2}$$

Where D_1 and D_2 are the diopters of th etwo original lenses. The distance from the center of equivalent lens to the display screen d_{ed} and the distance between lens and retina d_{er} satisfy Gaussian Thin Lens Equation in the form: $D = 1/f = 1/d_{ed} + 1/d_{er}$.

Here we demonstrate the modeling process with an actual example. A myopic eye that misfocuses objects onto the retina and requires a eyeglasses prescription of -5.00D, causes a

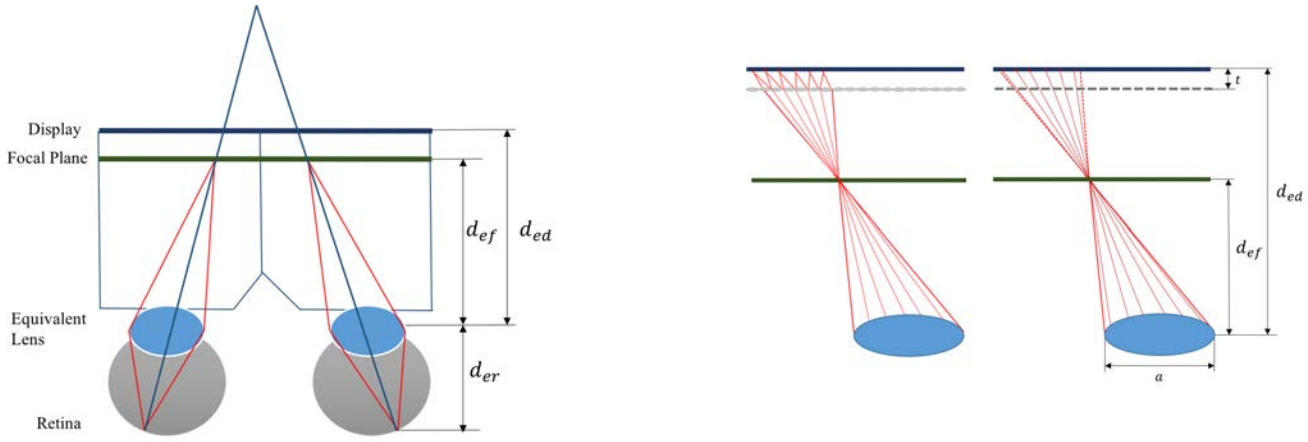

Figure 8.2: Schematics for single lens model approximation (left) and light field optical setup (right) using microlens array and pinhole aperture array

+5.00D diopter increase in the synthetic lens and brings the farthest focus plane closer to the eye according to the formula below:

$$D' \approx D + 5 = \frac{1}{f'} = \frac{1}{d_{ef}} + \frac{1}{d_{er}} \tag{8.3}$$

$$d_{ef} = \frac{d_{ed}}{5d_{ed} + 1} \tag{8.4}$$

The position of the plane of focus (d_{ef}), as is drawn green in Fig. 8.2, can be derived according to the position of display and input eye prescriptions.

8.4 Experiment Evaluation

In this work, we use a 6 mm clear acrylic plate to separate the pinhole array and the mobile display. The pinhole aperture array contains squared pinholes with 0.075 mm lengths of side and 0.39 mm center-to-center spacing as is shown in Fig. 8.3. A 6 mm pupil diameter is applied in the prefiltering algorithm as the average human pupil size, which equals to the size of eye box in our prototype. The distance d_{ed} from the display screen to the center of the synthetic lens is measured upon the Google Cardboard VR HMD. And the corresponding distance d_{ef} from the plane of focus to the lens of a -5.00D near-sighted eye is computed to be 33 mm as is shown in Table. 8.1.

A Nikon DSLR is used to capture the monocular perception of the rendered light field, by placing the camera in a distance that it can only focus on a plane in front of the actual

display panel. Both focal length and f-stop number are fixed and the exposure time is set to 2 seconds for higher brightness. Results are shown in Fig. 8.4 and Fig. 8.5.

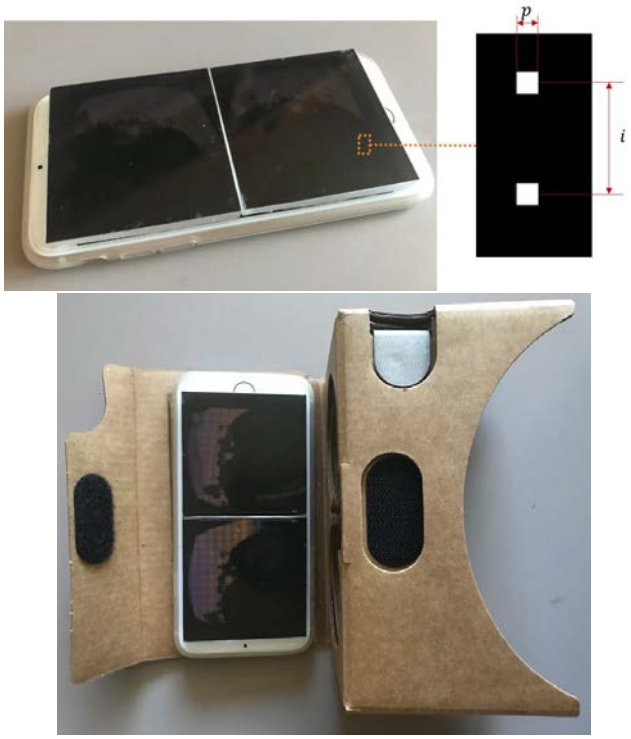

Figure 8.3: Experiment prototype with a pinhole array held by a 6 mm acrylic transparent plate on top of the display of mobile device, is placed inside the Google Cardboard to form a VR display system with visual correction.

Table 8.1: Parameter Setup

Parameter	Value	Parameter	Value
t	6 mm	p	75 μm
d_{ef}	46 mm	i	390 μm
d_{ed}	33 mm	a	6 mm

(a) Desired image perceived on retina

(b) Rendered content on display panel

(c) Blurry image observed without pinhole array

(d) Corrected image observed through pinhole array

Figure 8.4: Experiment results comparing visually corrected image (d) with blurry image observed with near-sighted eyes (c). Since the experiment is done with pinhole aperture array, the brightness loss may affect the visual comparison. Yet sharpness improvement is noticeable by comparing the fine detail such as the paws of the dinosaur fossil.

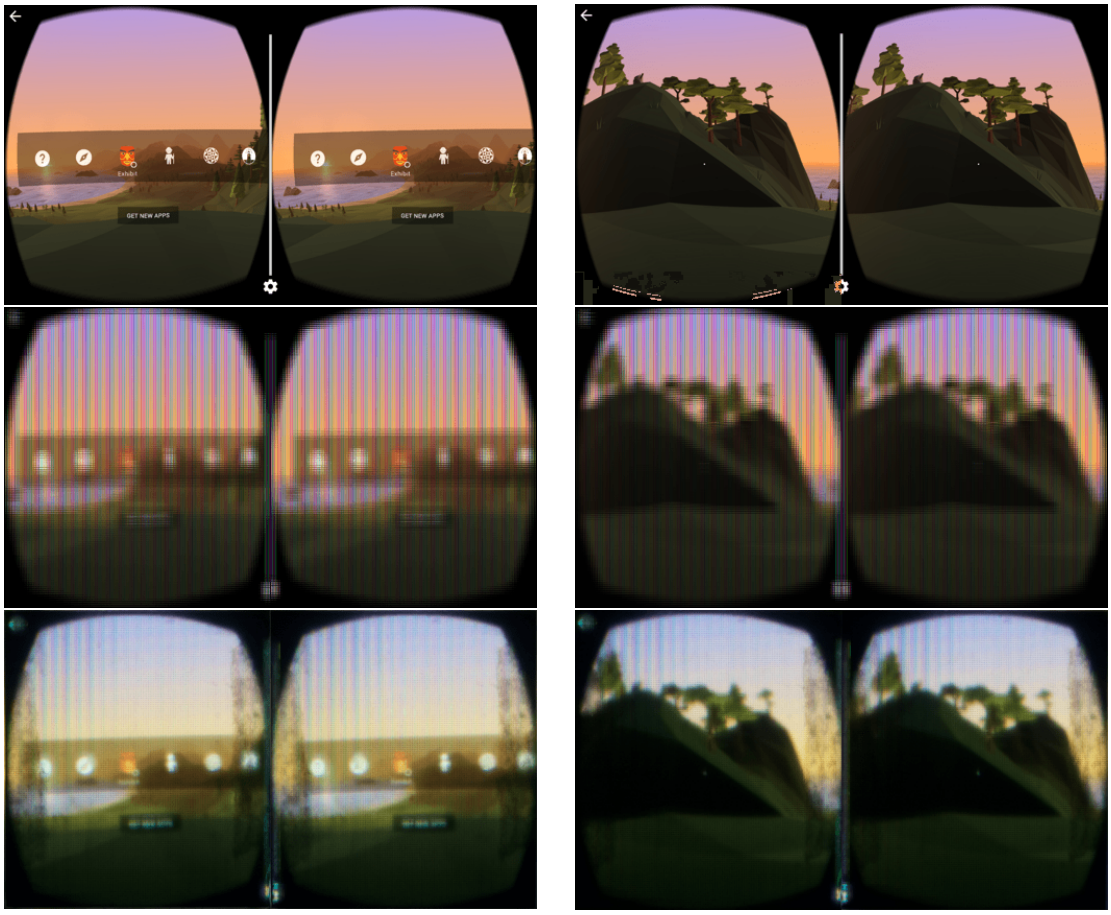

Figure 8.5: More experiment results evaluating the capability of vision correction of proposed method. Top row: desired sharp image pairs perceived on retina; Middle row: rendered inversely pre-blurred image pairs; Bottom row: corrected image pairs observed by DSLR through pinhole array.

Chapter 9

Conclusion and future work

Refractive visual aberrations including myopia, hyperopia, presbyopia, astigmatism, and other higher-order aberrations are proven to be widely experienced and are predicted to increase their prevalence in the future. The corrections for such visual impairments are extensively required, yet feasible solutions are primarily addressed by optical means. The eyeglasses, contact lenses and refractive surgery directly modify the optics of the eye and can sometimes be cumbersome. We introduce a computational solution for vision correcting purpose that has no direct contact with the eye.

9.1 Microlens Array Vision Correcting

In this work, we proposed the microlens array based light field pre-distortion rendering using the *forward* projection method. As opposed to the expensive ray tracing architecture in the Matlab implementation [17] that around 22000 rays across the pupil aperture were sampled, we showed a considerable quality reservation while significantly accelerate the runtime by keeping only one pupil sample per screen pixel.

We constructed and optimized the design of microlens array with Zemax. Theoretical limitations of the microlens array based light field display were analyzed. The light field pre-filtering and the software simulation were proposed to take the optical property of microlens array into consideration for higher brightness in comparison to the pinhole array light field display. The multi-sampling method was implemented to eliminate chromatic artifacts by sampling multiple points within the internal light emitting units of the screens. High contrast simulation results, physically captured images, and evaluations using HDR-VDP2 were demonstrated in the end.

The light field was rendered based on the approximation of thin lens eye model and in the regime of geometric optical ray tracing, which limited the ability to model complex wavefront geometry of light refracted by the visually impaired eye. Thus higher-order visual

aberrations are awaiting study. Leakage of light was the key causing contrast loss in our design. In the future, we can add barriers between different pinholes to prevent such issue. In this work, we proposed grid pattern microlens array, which could also be modified to a pattern with spatial-variant density allocation to increase the light reservation.

9.2 Vision Correcting in VR Head-Mounted Display

The application of the light field vision correcting display to the field of virtual reality head-mounted display was tested for the first time in this work. We built a low-cost pinhole aperture array based display prototype together with the refractive lenses in a commercial VR HMD – Google Cardboard. Physical experiment evaluation was carried out with the DSLR camera to demonstrate the capability of vision correcting in near eye immersive head-mounted display.

Our simplified single lens model was built upon the assumption that the viewer's eyes had close to 0 intervals from the magnifying lenses inside the VR HMDs, which can be further carefully modeled to achieve higher accuracy. The magnifying lenses used in the Google Cardboard have a thick form factor and cause additional optical aberrations, so in future works, we can further model lens-less VR HMDs using the light field display.

Bibliography

[1] Edward H Adelson and John YA Wang. "Single lens stereo with a plenoptic camera". In: *IEEE transactions on pattern analysis and machine intelligence* 14.2 (1992), pp. 99–106.

[2] Edward H Adelson, James R Bergen, et al. "The plenoptic function and the elements of early vision". In: (1991).

[3] Kaan Akşit, Jan Kautz, and David Luebke. "Slim near-eye display using pinhole aperture arrays". In: *Applied optics* 54.11 (2015), pp. 3422–3427.

[4] Kann Aksit, Jan Kautz, and David Luebke. "Slim near-eye display using pinhole aperture arrays". In: *Applied Optics* 54.11 (2015).

[5] Victor Delpizzo Castagno et al. "Hyperopia: a meta-analysis of prevalence and a review of associated factors among school-aged children". In: *BMC ophthalmology* 14.1 (2014), p. 163.

[6] Jin-Xiang Chai et al. "Plenoptic sampling". In: *Proceedings of the 27th annual conference on Computer graphics and interactive techniques*. ACM Press/Addison-Wesley Publishing Co. 2000, pp. 307–318.

[7] Charles Ding. "Algorithms and Applications of the Vision Correcting Display". MA thesis. EECS Department, University of California, Berkeley, May 2017. URL: `http://www2.eecs.berkeley.edu/Pubs/TechRpts/2017/EECS-2017-103.html`.

[8] Zernike von F. "Beugungstheorie des schneidenver-fahrens und seiner verbesserten form, der phasenkontrastmethode". In: *Physica* 1.7-12 (1934), pp. 689–704.

[9] RF Fisher. "Elastic constants of the human lens capsule". In: *The Journal of physiology* 201.1 (1969), pp. 1–19.

[10] Martin Fuchs et al. "Towards passive 6D reflectance field displays". In: *ACM Transactions on Graphics (TOG)* 27.3 (2008), p. 58.

[11] Howard V Gimbel et al. "Incidence and management of intraoperative and early postoperative complications in 1000 consecutive laser in situ keratomileusis cases". In: *Ophthalmology* 105.10 (1998), pp. 1839–1848.

[12] Adrian Glasser and Melanie CW Campbell. "Presbyopia and the optical changes in the human crystalline lens with age". In: *Vision research* 38.2 (1998), pp. 209–229.

[13] Rafael Gonzalez. "R. Woods Digital Image Processing". In: *Reading, MA: Addison-Welsley* (1992).

[14] Steven J Gortler et al. "The lumigraph". In: *Proceedings of the 23rd annual conference on Computer graphics and interactive techniques*. ACM. 1996, pp. 43–54.

[15] Hassan Hashemi et al. "Global and regional estimates of prevalence of refractive errors: Systematic review and meta-analysis". In: *Journal of Current Ophthalmology* (2017).

[16] BA Holden et al. "Global prevalence of myopia and high myopia and temporal trends from 2000 through 2050". In: *Ophthalmology* 123.5 (2016).

[17] Fu-Chung Huang. "A Computational Light Field Display for Correcting Visual Aberrations". PhD thesis. EECS Department, University of California, Berkeley, Dec. 2013. URL: `http://www2.eecs.berkeley.edu/Pubs/TechRpts/2013/EECS-2013-206.html`.

[18] Fu-Chung Huang et al. *Computational light field display for correcting visual aberrations*. ACM, 2013.

[19] F.-C. Huang, D. Lanman, and B.A. Barsky. "Correcting for optical aberrations using multilayer displays". In: *ACM Transactions on Graphics (SIGGRAPH Asia)*. Vol. 31. 6. 2012.

[20] F.-C. Huang, D. Lanman, and B.A. Barsky. "Near-eyelight field displays". In: *ACM Transactions on Graphics (SIGGRAPH Asia)*. Vol. 32. 6. 2013.

[21] T. Icenogle. *Wavefront-Guided LASIK*. `http://bme240.eng.uci.edu/students/08s/ticenogl/Wavefront-GuidedLASIK/Wavefront.html`. 2018.

[22] Aaron Isaksen, Leonard McMillan, and Steven J Gortler. "Dynamically reparameterized light fields". In: *Proceedings of the 27th annual conference on Computer graphics and interactive techniques*. ACM Press/Addison-Wesley Publishing Co. 2000, pp. 297–306.

[23] Frederic E Ives. *Parallax stereogram and process of making same*. US Patent 725,567. Apr. 1903.

[24] Nada S Jabbur, Keiko Sakatani, and Terrence P O'Brien. "Survey of complications and recommendations for management in dissatisfied patients seeking a consultation after refractive surgery". In: *Journal of Cataract & Refractive Surgery* 30.9 (2004), pp. 1867–1874.

[25] Jane F Koretz and George H Handelman. "Modeling age-related accomodative loss in the human eye". In: *Mathematical modelling* 7.5-8 (1986), pp. 1003–1014.

[26] Marc Levoy and Pat Hanrahan. "Light field rendering". In: *Proceedings of the 23rd annual conference on Computer graphics and interactive techniques*. ACM. 1996, pp. 31–42.

[27] Robert T Lin and Robert K Maloney. "Flap complications associated with lamellar refractive surgery". In: *American journal of ophthalmology* 127.2 (1999), pp. 129–136.

[28] Gabriel Lippmann. "Epreuves reversibles donnant la sensation du relief". In: *J. Phys. Theor. Appl.* 7.1 (1908), pp. 821–825.

[29] Rafat Mantiuk et al. "HDR-VDP-2: a calibrated visual metric for visibility and quality predictions in all luminance conditions". In: *ACM Transactions on graphics (TOG)*. Vol. 30. 4. ACM. 2011, p. 40.

[30] Wojciech Matusik and Hanspeter Pfister. "3D TV: a scalable system for real-time acquisition, transmission, and autostereoscopic display of dynamic scenes". In: *ACM Transactions on Graphics (TOG)*. Vol. 23. 3. ACM. 2004, pp. 814–824.

[31] Kovin S Naidoo et al. "Global vision impairment and blindness due to uncorrected refractive error, 1990–2010". In: *Optometry and Vision Science* 93.3 (2016), pp. 227–234.

[32] Ren Ng. *Digital light field photography*. stanford university California, 2006.

[33] Ren Ng et al. "Light field photography with a hand-held plenoptic camera". In: *Computer Science Technical Report CSTR* 2.11 (2005), pp. 1–11.

[34] V. Pamplona et al. "Tailored displays to compensate for visual aberrations". In: *ACM Transactions on Graphics*. Vol. 31. 2012.

[35] Donatella Pascolini and Silvio Paolo Mariotti. "Global estimates of visual impairment: 2010". In: *British Journal of Ophthalmology* 96.5 (2012), pp. 614–618.

[36] Ben C Platt and Roland Shack. "History and principles of Shack-Hartmann wavefront sensing". In: *Journal of Refractive Surgery* 17.5 (2001), S573–S577.

[37] Ronald A Schachar. "The mechanism of accommodation and presbyopia in the primates". In: *Ann Ophthalmol* 27 (1995), pp. 58–67.

[38] Clifton M. Schor. *Oculomotor Fundcions and Neurology*. University of California, Berkeley, School of Optometry, 1997.

[39] Market Scope. *Global Presbyopia-Correcting Surgery Market Report*. 2012.

[40] R Doyle Stulting et al. "Complications of laser in situ keratomileusis for the correction of myopia". In: *Ophthalmology* 106.1 (1999), pp. 13–20.

[41] Sijia Teng, Jia Zeng, and Vivek Claver. "Vision Correcting Display - Master of Engineering Capstone Final Report". MA thesis. EECS Department, University of California, Berkeley, May 2017. URL: `http://www2.eecs.berkeley.edu/Pubs/TechRpts/2017/EECS-2017-96.html`.

[42] Larry N Thibos, Arthur Bradley, and Xin Hong. "A statistical model of the aberration structure of normal, well-corrected eyes". In: *Ophthalmic and Physiological Optics* 22.5 (2002), pp. 427–433.

[43] Hakan Urey et al. "State of the art in stereoscopic and autostereoscopic displays". In: *Proceedings of the IEEE* 99.4 (2011), pp. 540–555.

[44] S Vitale, R.D. Sperduto, and F.L. Ferris III. *Increased prevalence of myopia in the United States between 1971-1972 and 1999-2004*. 2009.

[45] T.Y. Wong et al. *Prevalence and risk factors for refractive errors in adult chinese in singapore*. 2000.

[46] William David Wright. "A re-determination of the trichromatic coefficients of the spectral colours". In: *Transactions of the Optical Society* 30.4 (1929), p. 141.

[47] Zehao Wu. "Investigating Computational Approaches and Proposing Hardware Improvement to the Vision Correcting Display". MA thesis. EECS Department, University of California, Berkeley, May 2016. URL: `http://www2.eecs.berkeley.edu/Pubs/TechRpts/2016/EECS-2016-67.html`.

[48] Jeff Yurek. *Color Space Confusion*. `https://dot-color.com/2012/08/14/color-space-confusion/`. August, 14, 2012.

[49] Matthias Zwicker et al. "Antialiasing for automultiscopic 3D displays". In: *ACM SIGGRAPH 2006 Sketches*. ACM. 2006, p. 107.